A field investigation into the effects of a kelp forest (*Macrocystis pyrifera*) on coastal hydrodynamics and transport

Johanna H. Rosman,[1] Jeffrey R. Koseff,[1] Stephen G. Monismith,[1] and Jamie Grover[2]

Received 2 December 2005; revised 24 July 2006; accepted 3 October 2006; published 16 February 2007.

[1] *Macrocystis pyrifera* (Giant Kelp) forests form important habitats in temperate coastal regions. Hydrodynamics control the transport of nutrients, food particles, larvae and spores at scales ranging from boundary layers around individual blades to entire kelp forests. Our measurements include vertical profiles of current and temperature, and concurrent wave measurements, at a number of different locations in and around a kelp forest at Santa Cruz, California. We find that flow at the site is dominated by variations at diurnal and semidiurnal frequencies. A vertically sheared across-shore flow, consistent with flow driven by an across-shore density gradient, is thought to be important for exchange between the kelp forest and the surrounding coastal ocean. Within the kelp forest, currents are reduced by a factor that correlates with surface canopy coverage, higher frequency internal waves are damped, and onshore transport due to waves (Stokes drift) is estimated to be similar in magnitude to that due to currents. Richardson numbers within the kelp forest are higher than those outside the kelp forest and indicate that the water column within the kelp forest is usually stable to turbulence generation by mean velocity shear.

Citation: Rosman, J. H., J. R. Koseff, S. G. Monismith, and J. Grover (2007), A field investigation into the effects of a kelp forest (*Macrocystis pyrifera*) on coastal hydrodynamics and transport, *J. Geophys. Res.*, *112*, C02016, doi:10.1029/2005JC003430.

1. Introduction

[2] Subtidal rocky environments in temperate nearshore regions are generally dominated by large brown algae of the order Laminariales, more commonly known as kelps. In the northeast Pacific, off the coast of California, Giant Kelp (*Macrocystis pyrifera*) form forests that are home to diverse assemblages of organisms. Such kelp forests are also found along the southern shores of South America, islands of the Southern Ocean and parts of South Africa, Australia and New Zealand [*Dayton*, 1985].

[3] Macrocystis forests typically occupy areas of rocky substrate between 7 and 20 m deep. The kelp is attached to the rocky substrate by a root-like holdfast which anchors anywhere from one to 200 or more individual fronds (stipes plus attached blades). Fronds, buoyed by gas bladders (pneumatocysts), intertwine and extend towards the surface forming bundles that are typically between 10 cm and 40 cm in diameter (J. Grover, personal communication). Within a kelp forest typical kelp densities range from 1 to 15 individuals per 100 m^2. Fronds can reach 45 m in length and spread out upon reaching the surface to form a dense canopy in the top meter of the water column [*Utter and Denny*, 1996; *Langstroth and Langstroth*, 2000].

[4] Hydrodynamics are important for the functioning of kelp forest ecosystems, both at the scale of an entire kelp forest and at the scale of an individual organism or group of organisms. *Graham* [2003] found that within the Point Loma kelp forest, off San Diego, California, Macrocystis spore supply was closely coupled with the local adult density, whereas the correlation between spore supply and adult density near the kelp forest edges was much weaker. He hypothesized that the edges of the kelp forest were subject to large mean velocities, leading to potentially large displacements of spores between release from an adult and settlement, while within the kelp forest currents were reduced, leading to much smaller dispersal distances. The vertical movement of particles such as spores and larvae can be affected by surface waves, internal waves and vertical turbulent mixing as well as swimming behavior. Exchange between a kelp forest and the surrounding coastal ocean can be driven by many processes; for example, sustained wind-driven upwelling, internal waves [*Zimmerman and Kremer*, 1984; *Piñeda*, 1994], and submesoscale coastal eddies [*Bassin et al.*, 2005] are all thought to be important mechanisms for transport of nutrients and larvae from offshore to inner shelf ecosystems such as kelp forests.

[5] To our knowledge, there have been no documented measurements of the flow field within Giant Kelp forests since Jackson's measurements in the Point Loma kelp bed in southern California in the early 1980s [*Jackson and Winant*, 1983; *Jackson*, 1984, 1998]. Jackson's work iden-

[1] Environmental Fluid Mechanics Laboratory, Civil and Environmental Engineering, Stanford University, Stanford, California, USA.
[2] Institute of Marine Sciences, University of California, Santa Cruz, California, USA.

Copyright 2007 by the American Geophysical Union.
0148-0227/07/2005JC003430

tified a number of important aspects of the hydrodynamics within kelp forests. The average magnitude of the near-surface alongshore current was reduced by a factor of up to 5 within the kelp forest. Based on kelp forest dimensions in the alongshore and across-shore directions, and excursion lengths (maximum particle displacements during one flow cycle) estimated from velocity measurements, Jackson concluded that across-shore transport was likely to be more important than alongshore transport for exchange of materials between the kelp forest and the surrounding coastal ocean [*Jackson*, 1998].

[6] Records of temperature taken during Jackson's experiments had spectral peaks at diurnal and semidiurnal frequencies and a high coherence with across-shore velocity at these timescales, suggestive of low frequency internal waves propagating onshore [*Jackson*, 1984]. *Lerczak et al.* [2003] described intermittent semidiurnal internal tides on the shelf immediately offshore of the Point Loma kelp bed, and attributed their observations to a partially reflected mode one internal wave, supporting Jackson's findings. Tidal band velocity variations off the coast of Northern California, between Point Reyes and Point Arena, 150–300 km north of Santa Cruz, were examined in detail in a series of papers by Rosenfeld [*Rosenfeld and Beardsley*, 1987; *Rosenfeld*, 1988, 1990]. These papers identified (a) diurnal temperature and velocity variations that were attributed to diurnal wind stress in combination with diurnal tidal currents [*Rosenfeld*, 1988], (b) barotropic semidiurnal currents, related to semidiurnal tides modulated by local small-scale topography [*Rosenfeld*, 1988], and (c) baroclinic semidiurnal currents consistent with a partially reflected wave first mode internal wave [*Rosenfeld*, 1990], similar to those described by *Lerczak et al.* [2003] in Southern California. *Piñeda* [1994], *Leichter et al.* [1996, 1998], and others have shown that internal motions like (a) and (c) may be important for the onshore transport of nutrients and larvae on the shelf break and inner shelf.

[7] Trains of high frequency internal waves are frequently observed in association with internal tides in coastal regions. S. Venayagamoorthy and O. Fringer (Energetics of the interaction of internal gravity waves with a shelf break, submitted to *Journal of Fluid Mechanics*, 2006) performed numerical simulations of the interaction of a low frequency internal wave with a shelf and slope topography and observed a bolus feature that propagated shoreward, like a density current across the shelf. High frequency internal waves have been observed to form on the front faces of these bores due to nonlinear steepening, but because of their slower propagation speeds, higher frequency internal waves are typically observed behind the head of the bore in the near-shore [*Colosi et al.*, 2001; *Piñeda*, 1994; *Storlazzi et al.*, 2003]. Within the Point Loma kelp bed, *Jackson* [1984] found evidence that high frequency internal waves were damped, and the phase speed of lower frequency internal waves was reduced, suggesting that the kelp bed acted as a sink for internal wave energy. However, the vertical structure of these variations was not documented and as the sampling interval was 4 min, the high frequency end of the internal wave spectrum was not well resolved.

[8] Kelp forests generally grow in regions affected by surface waves. In an experiment off Carlsbad, California, *Elwany et al.* [1995] found that wave properties inshore of a kelp forest were not significantly altered from those at a comparable site without kelp, indicating that the kelp forest caused negligible damping of surface waves at measurable frequencies (0.3 Hz and less). Nonlinear wave effects can result in a net transport in the direction of wave propagation (Stokes drift) that can affect the forces experienced by flexible organisms such as kelp [*Gaylord et al.*, 2003], and enhance across-shelf transport beyond that due to mean currents alone [*Longuet-Higgins*, 1953; *Monismith and Fong*, 2004]. Thus, waves may be important for onshore transport in kelp forests.

[9] The present study aims to assess the relative importance of different hydrodynamic processes for exchange between a kelp forest and the surrounding environment, and to identify the effect of a kelp forest on local hydrodynamics, building on the previous work described above. Two experiments were performed at Terrace Point, in Santa Cruz, California, in May and October 2003. Our measurements include vertical profiles of current and temperature and concurrent wave measurements at a number of different locations in and around the kelp forest, offering a more detailed picture of kelp forest hydrodynamics than has been available in the past. Our findings are divided into two parts, a description of the flow environment immediately outside the kelp forest, with emphasis on the processes that may be important for exchange (section 4), and an analysis of the effect of a kelp forest on these processes (section 5).

2. Background on the Field Site

[10] The site of the field study was Terrace Point in Santa Cruz, California, at the northern end of Monterey Bay. The site was chosen for its relatively simple, straight coastline and low relief (order of 20 cm) bottom topography. Figure 1 shows the location of the field site relative to Monterey Bay and more detailed bathymetry of the Terrace Point and Natural Bridges area, along with kelp canopy coverage from aerial surveys conducted by the California Department of Fish and Game in 2002. Aerial images were taken by the Department of Fish and Game at this site in late October of 2002 and 2003, but the canopy coverage is more complete in the 2002 survey results. This is likely a reflection of true variations in kelp canopy coverage, as well as apparent differences in kelp canopy coverage due to water depth and currents at the time of imaging, and image quality. As the 2002 survey gives a better representation of the extent of the canopy observed throughout the summer months of 2003, it is shown in Figure 1 in preference to the 2003 survey results. This figure is included solely to indicate the instrument locations relative to the shoreline, local bathymetry, and kelp forest. For a more accurate representation of the surface canopy coverage during the experiments, see Figure 7.

[11] The time-averaged surface circulation in Monterey Bay has been characterized by a counterclockwise eddy, with occasional flow reversals that can last several days [*Breaker and Broenkow*, 1994]. *Drake et al.* [2005] and *Storlazzi et al.* [2003] observed the mean flow at Terrace Point, and at Sand Hill Bluff, 9 km WNW of Terrace Point, to be predominantly northwest, out of the bay. This is in direct opposition to the local wind stress, which is usually toward the southeast, suggesting an alongshore pressure gradient force directed out of the bay [*Drake et al.*, 2005].

21562202c, 2007, C2, Downloaded from https://agupubs.onlinelibrary.wiley.com/doi/10.1029/2005JC003430 by University Of North Carolina W, Wiley Online Library on [17/09/2024]. See the Terms and Conditions (https://onlinelibrary.wiley.com/terms-and-conditions) on Wiley Online Library for rules of use; OA articles are governed by the applicable Creative Commons License

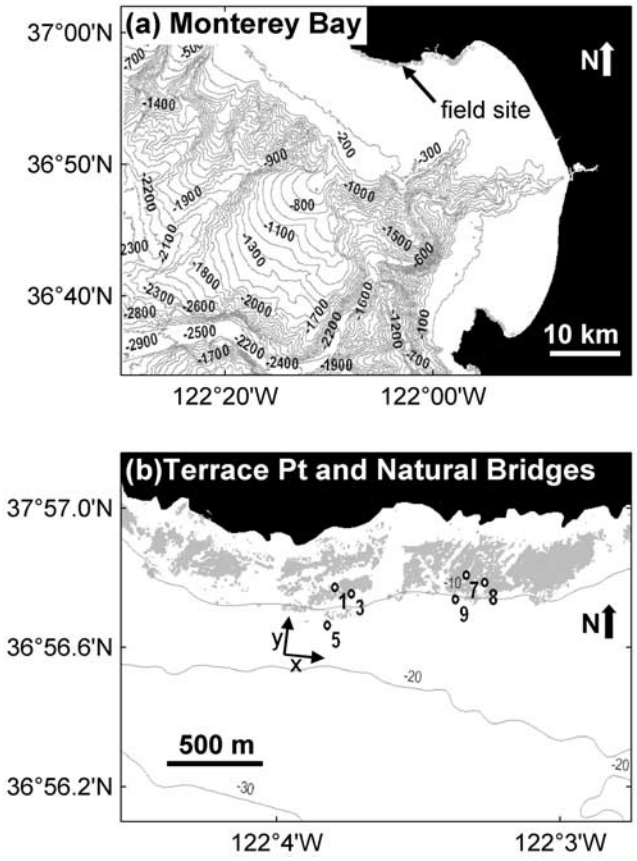

Figure 1. Maps showing the location of the field site. (a) Map of Monterey Bay with depth contours at 100 m intervals. (b) Map of the Terrace Point and Natural Bridges area with depth contours at 10 m intervals and instrument locations numbered. Positive alongshore (x) and across-shore (y) are indicated by the axes close to location 5. Land area is colored black, and grey represents areas that were classified as "kelp canopy" during aerial surveys conducted in 2002 by the California Department of Fish and Game.

[12] *Storlazzi et al.* [2003] have found the temperature and velocity spectra during the spring and summer at Sand Hill Bluff to be dominated by variations at semidiurnal and diurnal frequencies, with associated packets of high frequency internal waves. The velocity and temperature fields are suggestive of internal tidal bores propagating onshore. A number of studies have measured high energy internal tides in the Monterey Bay submarine canyon [*Petruncio et al.*, 1998; *Kunze et al.*, 2002], and field [*Kunze et al.*, 2002] and numerical [*Jachec et al.*, 2006] studies have identified regions of the canyon as potential generation sites for internal tides. It is thought that these internal tides could result in the periodic pumping of cool water onto the shallow regions on either side of the canyon [*Petruncio et al.*, 1998], which may then propagate across the shallow shelf as bores, such as those observed by *Storlazzi et al.* [2003].

[13] These papers illustrate the complex nature of flow in the shallow coastal ocean within Monterey Bay. Flow at the Terrace Point site is likely determined by local and regional wind stress, surface tides, and locally and remotely generated internal tides, all heavily modified by the local bathymetry. Additionally, swell and wind waves may influence the circulation at the site.

3. Methods

[14] Instrument positions and programming parameters for the two experiments are summarized in Table 1. The May deployment (8 May through 29 May 2003) focused on the kelp patch directly off Terrace Point. The October deployment was divided into two approximately two-week long phases: phase 1 (28 September through 11 October) focused on the higher density kelp region off Natural Bridges, 0.7 km to the east of Terrace Point, and phase 2 (11–29 October) focused on the low kelp density region off Terrace Point, with some instruments left in place for the full four weeks to allow comparison between the two sites. For both experiments, Acoustic Doppler Current Profilers (Workhorse, RD Instruments) were mounted on the bottom, looking upwards, and obtained velocity profiles at 1 min intervals with a standard deviation of 2 cm/s or less. The bin size was 0.5 m in all cases except for the ADCP at location 5 during the May deployment, which had a bin size of 1 m. Thermistor strings were composed of either Seabird (SBE39) thermistors, (accuracy 0.01°C, resolution 0.0001°C, response time 0.5 s) or Onset Computer Corporation's StowAway XTI with a 4″ stainless steel probe (accuracy 0.4°C, resolution 0.2°C, response time constant 6.5 s). Wave gauges (Seabird SBE26) were mounted close to the bottom and recorded pressure to an accuracy of 5 mm for wave and tide measurements.

[15] Aerial photographs of the site were taken during each of the two experiments in order to compare surface canopy coverage between experiments and identify instrument locations relative to the kelp canopy. These photographs were subdivided into overlapping 128 × 128 pixel subwindows, corresponding to 18 m by 18 m subwindows for the photograph taken during the May deployment and 14 m by 14 m subwindows for the photographs taken during the October deployment. Individual pixels were classified according to coloration as either kelp or nonkelp areas, and percent surface coverage was calculated over each subwindow. Additionally, to characterize average kelp spacings, numbers of kelp individuals were counted along transects by divers. Only individuals having heights greater than 1 m were included in these counts. In May, kelp were counted along eight 30 m by 4 m transects and three 50 m by 2 m transects. In October, kelp were counted along eight 50 m by 2 m transects.

4. Flow Conditions During the Experiment

4.1. An Overview of the Variability

[16] During both experiment periods, the wind measured at the National Data Buoy Center (NDBC) buoy 46042, 50 km west of Monterey Bay (36°45′N,122°25′W), was upwelling favorable, predominantly from the northwest. We were unable to obtain local wind measurements for full 24 hour cycles for the duration of the experiments; however, during the spring and summer months winds typically exhibit a diurnal cycle. Winds are weak and variable in direction in the early morning, increase to become strong and westerly in the late morning/early afternoon, and

21562202c, 2007, C2, Downloaded from https://agupubs.onlinelibrary.wiley.com/doi/10.1029/2005JC003430 by University Of North Carolina W, Wiley Online Library on [17/09/2024]. See the Terms and Conditions (https://onlinelibrary.wiley.com/terms-and-conditions) on Wiley Online Library for rules of use; OA articles are governed by the applicable Creative Commons License

Table 1. Instrument Positions and Programming Parameters for Each Deployment Period: 8–29 May 2003 (May Deployment), 28 September Through 11 October 2003 (October Deployment, Part I), and 11–29 October 2003 (October Deployment, Part II)

Location, Depth	May	October (Part I)	October (Part II)	Notes
1 36°56′46″N, 122°03′49″W depth 8.3 m	ADCP (1200 kHz) wave-tide gauge (SBE26)		ADCP (600 kHz) wave-tide gauge (SBE26)	45 pings per 1-min ensemble 0.5 m bins tide every 30 min, waves (for 8.5 min) every 2 hrs (May) and 3 hrs (Oct)
3 36°56′45″N, 122°03′45″W depth 9.2 m	ADCP (1200 kHz) thermistors (SBE39)		ADCP (1200 kHz)	45 pings per 1-min ensemble 0.5 m bins 1, 2, 3, 5 m above bottom sampling interval 40 s
5 36°56′39″N, 122°03′50″W depth 13.7 m	ADCP (600 kHz)	ADCP (600 kHz) thermistors (XTI)	ADCP (600 kHz) thermistors (XTI)	45 pings per 1-min ensemble 1 m bins (May), 0.5 m bins (Oct) 2, 4, 6, 8, 10, 11 m above bottom sampling interval 60 s
7 36°56′48″N, 122°03′21″W depth 8.9 m		ADCP (1200 kHz) thermistors (SBE39)	 thermistors (SBE39)	45 pings per 1-min ensemble 0.5 m bins 1, 2, 3, 4, 5, 6 m above bottom sampling interval 60 s
8 36°56′47″N, 122°03′16″W depth 8.7 m		wave-tide gauge (SBE26)		tide every 30 min, waves (2 Hz for 8.5 min) every 3 hrs
9 36°56′44″N, 122°03′23″W depth 11.8 m		thermistors (SBE39) ADCP (1200 kHz) wave-tide gauge (SBE26)	thermistors (SBE39) ADCP (1200 kHz) wave-tide gauge (SBE26)	1, 2, 3, 4, 5, 6, 7 m above bottom. sampling interval 60 s 45 pings per 1-min ensemble 0.5 m bins tide every 30 min, waves (2 Hz for 8.5 min) every 3 hrs

decrease again in the late afternoon or early evening. We were able to obtain wind measurements from Long Marine Laboratory during the experiments for the hours of noon–5:30 pm, the time of day when winds are typically strongest. During these hours, winds were consistently from the west with a mean wind speed of 28.6 km/h in May and 18.4 km/h in October.

[17] Velocity and temperature measurements at location 5 gave an indication of the flow field in the shallow coastal ocean offshore of the kelp forest. The alongshore direction was deduced by finding the principal axes of depth-averaged velocities over each deployment period. The alongshore direction, defined to be the direction of maximum variance in the depth-averaged velocity at a given measurement location, was within 15° of east-west at location 5 for both experiments. The alongshore (x) and across-shore (y) directions are indicated by axes marked on Figure 1b.

[18] Figures 2 and 3 show currents, water temperatures and wave conditions during May and October, respectively. For both the May and October measurement periods, currents exhibit (1) a nonzero mean, (2) a subtidal frequency band between the frequencies 0.13 d^{-1} and 0.51 d^{-1}, (3) dominant peaks at semidiurnal and diurnal frequencies in the tidal band (0.51 d^{-1} to 2.2 d^{-1}), and (4) some energy at higher frequencies (> 2.2 d^{-1}). In order to determine the variability in each of these frequency ranges, time series of depth averaged velocity and top to bottom velocity difference, as well as depth average temperature and top to bottom temperature difference, were filtered using 3rd order Butterworth band-pass filters. The means and standard deviations of velocity and temperature within the above mentioned frequency bands are reported in Table 2.

[19] The mean flow was alongshore toward the west, out of the bay, and was slightly stronger in May (7.2 cm/s at 5° offshore) compared with October (5.9 cm/s at 1° offshore). This agrees with previous observations at the site [*Storlazzi et al.*, 2003; *Drake et al.*, 2005], and with the counterclockwise spring and summer circulation in Monterey Bay described in the literature [*Breaker and Broenkow*, 1994]. Subtidal and tidal band alongshore velocity variations were a factor of two larger in May than in October. Across-shore flows were highly sheared, usually onshore in one part of the water column and offshore in the other part of the water column, and depth-averaged across-shore velocities were small during both deployments. Across-shore velocity shear in the tidal band was 25% less in October than in May. The energy at higher frequencies was similar between the two deployments.

[20] Temperature fluctuations were similar for the two deployments, showing variations at tidal frequencies of 2–4°C over the entire water column, although temperatures were 2°C warmer on average in October than in May. In addition to these low frequency variations, temperature spectra from measurements outside the kelp forest show a band of temperature fluctuations with periods between 5 min and 1 hour. This internal wave band is bounded at the high frequency end by the Brunt-Väisälä frequency, which is typically between 0.0017 and 0.0033 Hz (corresponding to 5–10 min period). The internal waves were present during periods of high stratification that typically followed semi-

21562202c, 2007, C2, Downloaded from https://agupubs.onlinelibrary.wiley.com/doi/10.1029/2005JC003430 by University Of North Carolina W, Wiley Online Library on [17/09/2024]. See the Terms and Conditions (https://onlinelibrary.wiley.com/terms-and-conditions) on Wiley Online Library for rules of use; OA articles are governed by the applicable Creative Commons License

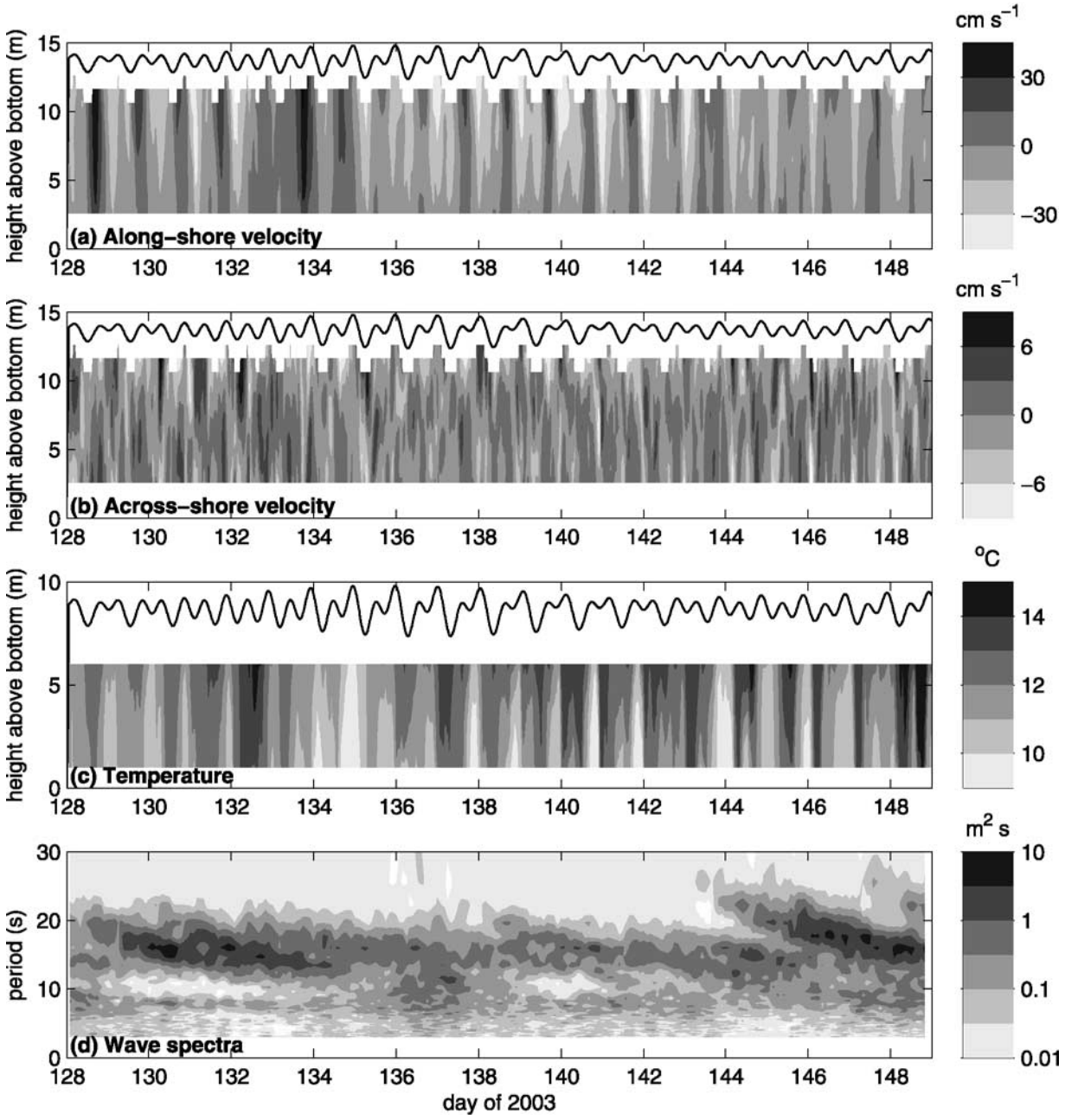

Figure 2. Conditions during the May deployment (8 May through 29 May 2003). Plots are time series of (a) alongshore velocity (positive eastward) and (b) across-shore velocity (positive northward, onshore) at location 5, (c) temperature at location 3, and (d) wave spectra at location 1. Velocities and temperatures are 90-min smoothed data. Wave spectra are averages over 6-hour periods.

diurnal and diurnal warming or cooling events in both May and October. The associated velocity and temperature fluctuations were characteristic of a first mode internal wave, with vertical velocities up to 2 cm/s and isopycnal displacements reaching 4 m.

[21] During both May and October, the wave field was characterized by bands of swell with periods of 12–20 s and higher frequency wind waves with periods of 6 to 10 s (Figures 2e and 3e). The wind wave peak was significantly larger during May than during October. Significant wave heights [*Dean and Dalrymple,* 1991] varied between 0.5 m and 1.5 m for both experiments. The mean significant wave height in May was 0.77 m (standard deviation 0.19 m) and the mean significant wave period was 11.3 s (standard deviation 2.4 s), measured in 8.2 m of water at location 1. During October, the mean significant wave height and period were 0.87 m (standard deviation 0.32 m) and 11.8 s (standard deviation 2.5 s), respectively, measured in 11.7 m of water at location 9. Unfortunately we did not have wave measurements at the same location for the full duration of both experiments, but significant wave heights and periods at location 1 and 9 were quite similar during the week in

21562202c, 2007, C2, Downloaded from https://agupubs.onlinelibrary.wiley.com/doi/10.1029/2005JC003430 by University Of North Carolina W, Wiley Online Library on [17/09/2024]. See the Terms and Conditions (https://onlinelibrary.wiley.com/terms-and-conditions) on Wiley Online Library for rules of use; OA articles are governed by the applicable Creative Commons License

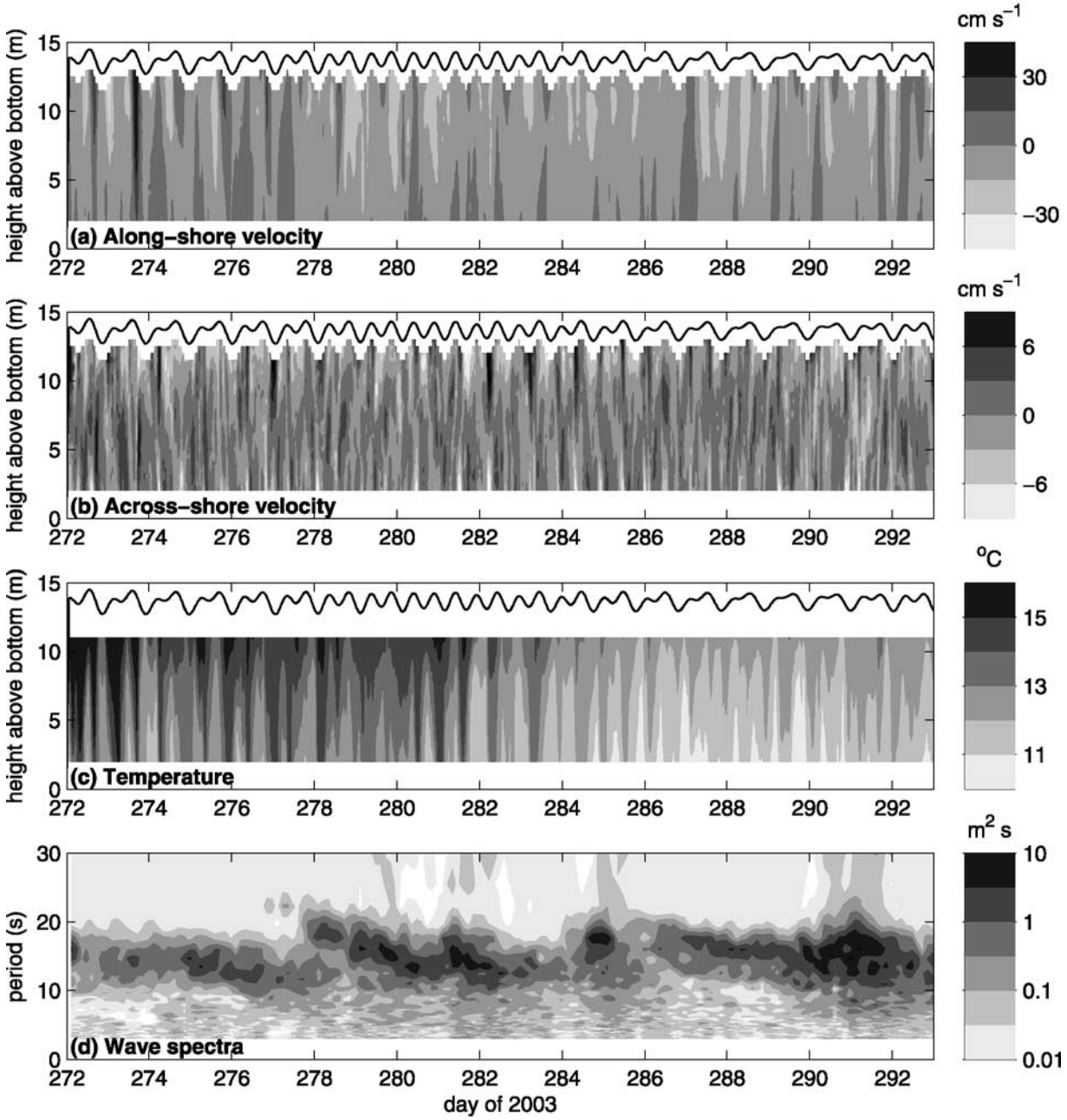

Figure 3. Conditions during the October deployment (29 September through 20 October 2003). Plots are time series of (a) alongshore velocity (positive eastward) and (b) across-shore velocity (positive northward, onshore) at location 5, (c) temperature at location 5, and (d) wave spectra at location 9. Velocities and temperatures are 90-min smoothed data. Wave spectra are averages over 6-hour periods.

October when simultaneous measurements were obtained at both locations.

4.2. Tidal Band Variability

[22] The semidiurnal and diurnal temperature and velocity signals at Terrace Point may result from (a) diurnal wind stress, (b) local surface tides, (c) locally generated internal tides or (d) shoreward propagation of internal tides generated further offshore, possibly within the Monterey Bay canyon region (refer to section 2). In order to further investigate the relationship between currents, temperatures and tides at this site, the velocity and temperature time series were decomposed using principal component analysis (Empirical Orthogonal Functions). In this analysis, alongshore and across-shore components of velocity were treated separately. Time-mean profiles were subtracted from velocity measurements, and time series were hourly-averaged and detrended using a high pass Butterworth filter with a cutoff frequency of 0.33 d^{-1}. Empirical orthogonal functions were then computed as the eigenvectors of the covariance matrix.

[23] The principal modes of velocity and temperature are shown in Figure 4, along with spectra of the modal

21562202c, 2007, C2, Downloaded from https://agupubs.onlinelibrary.wiley.com/doi/10.1029/2005JC003430 by University Of North Carolina W, Wiley Online Library on [17/09/2024]. See the Terms and Conditions (https://onlinelibrary.wiley.com/terms-and-conditions) on Wiley Online Library for rules of use; OA articles are governed by the applicable Creative Commons License

Table 2. Statistics of Depth-Averaged Alongshore and Across-Shore Velocities and Temperatures (U, V, T), and Vertically Differenced Alongshore and Across-Shore Velocities and Temperatures (ΔU, ΔV, ΔT), Calculated Over the May Deployment and the October Deployment[a]

	U, cm s^{-1}	ΔU, cm s^{-1}	V, cm s^{-1}	ΔV, cm s^{-1}	T, °C	ΔT, °C
			May			
Mean	−7.2	−4.3	−0.6	−0.7	11.8	1.0
Subtidal	6.0	3.2	0.4	1.0	1.9	0.4
Tidal	10.7	8.6	0.7	3.5	1.0	0.4
High	3.9	4.9	1.0	3.5	0.5	0.4
			October			
Mean	−5.9	−5.0	−0.1	−0.2	12.8	1.3
Subtidal	3.2	2.4	0.4	0.7	1.8	0.4
Tidal	5.0	5.1	0.6	2.7	0.9	0.4
High	3.3	4.4	0.9	3.8	0.5	0.4

[a]Velocities were measured at location 5, temperatures in May were measured at location 3, and temperatures in October were measured at location 5. ΔU and ΔV are the average of the top 3 m of velocity measurements minus the average of the bottom 3 m of velocity measurements. ΔT is the difference between the top and bottom temperature measurements. Standard deviations are given within three frequency bands: subtidal (<0.13 d^{-1}), tidal (0.51–2.2 d^{-1}), and high frequency (>2.2 d^{-1}).

amplitudes for the May and October experiments. The first modes of alongshore and across-shore velocity and temperature were nearly identical between experiments. The first mode of alongshore velocity was unidirectional over the water depth and accounted for 94% of the alongshore velocity variance in May and 84% of the alongshore velocity variance in October. The first mode of across-shore velocity was a sheared flow that was onshore in one half of the water column and offshore in the other half of the water column. This mode accounted for 55% of the across-shore variance in May and 56% of the across-shore variance in October. The first mode of temperature corresponded with a warming, or cooling, of the entire water column. This mode accounted for 94% of the temperature variance in May and 81% of the temperature variance in October. Spectra of the first modes of velocity and temperature in May all exhibit a dominant peak at the diurnal frequency and a smaller peak at the semidiurnal frequency. In October, variability at the semidiurnal frequency was similar to that in May, but the variability at the diurnal frequency was reduced substantially.

[24] Correlation coefficients and lags between the dominant modes are summarized in Table 3, and the two main flow states deduced from these correlations are depicted schematically in Figure 5. Correlations between 2nd and higher modes were weak ($r < 0.4$) in all cases and have been omitted from this discussion. In May, there was a correlation at zero phase lag between the first modes of alongshore and across-shore velocity. When flow was onshore at the surface and offshore at the bottom, alongshore flow was toward the west, and vice versa. Temperature lagged velocity by 3.5–4 hours. Onshore flow at the surface corresponded to periods of warming (lowering isopycnals), onshore flow at depth corresponded to periods of cooling (rising isopycnals). In May, the maximum eastward alongshore velocity, and maximum offshore flow at the surface and onshore flow at

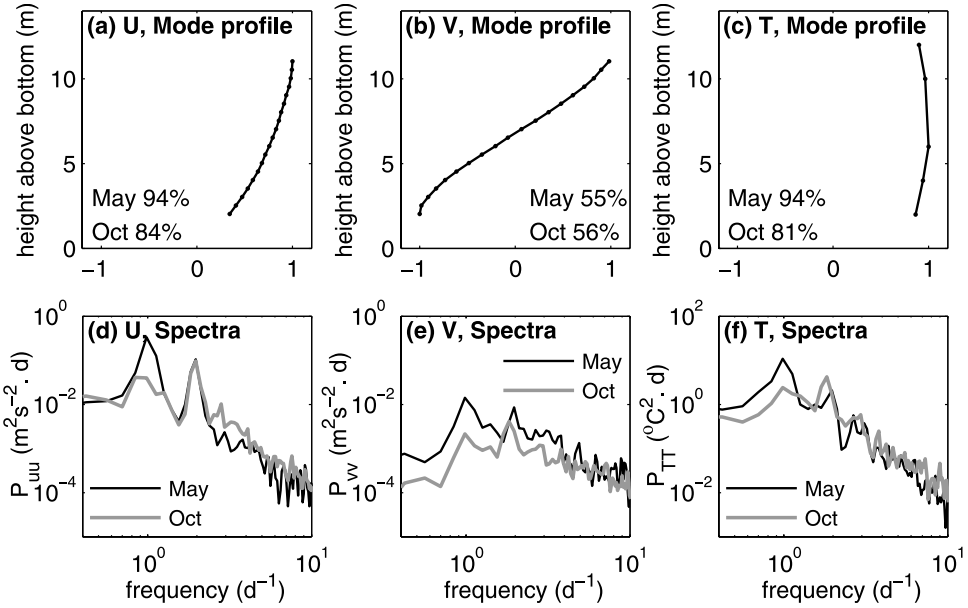

Figure 4. Results from Principal Component Analysis of velocities and temperatures at location 5, outside the kelp forest. The first row shows the mode profiles corresponding to the first mode of (a) alongshore velocity (u), (b) across-shore velocity (v), and (c) temperature (T) and the percentage of the total variance accounted for by the first mode. The shapes of the mode profiles were very similar in May and October and thus only the October modes are shown here. Mode profiles have been normalized such that the maximum positive or negative value is 1. The second row of the figure shows spectra of the modal amplitude time series, which have units of velocity and describe the way in which the vertical modes vary in time, for (d) alongshore velocity, (e) across-shore velocity and (f) temperature in May (black) and October (grey).

21562202c, 2007, C2, Downloaded from https://agupubs.onlinelibrary.wiley.com/doi/10.1029/2005JC003430 by University Of North Carolina W, Wiley Online Library on [17/09/2024]. See the Terms and Conditions (https://onlinelibrary.wiley.com/terms-and-conditions) on Wiley Online Library for rules of use; OA articles are governed by the applicable Creative Commons License

Table 3. Correlations Between the Modal Amplitude Time Series for the First Modes of Velocity and Temperature From Principal Component Analysis[a]

	Tide	U, Mode 1	V, Mode 1
	May		
U, mode 1	−0.48, 5.5 hr		
V, mode 1	0.35, 5.5 hr	−0.56, 0 hr	
T, mode 1	0.43, 8.2 hr	−0.60, 4 hr	0.49, 3.5 hr
	October		
U, mode 1	N/A		
V, mode 1	N/A	N/A	
T, mode 1	N/A	N/A	0.42, 1.7 hr

[a]Cell format is (*r*, *lag*) where *r* is the correlation coefficient and *lag* is the lag between the two time series at which the correlation coefficient is a maximum. Correlations less than 0.3 have been omitted. Positive lag means that the quantity in the top row leads the quantity in the first column.

depth, occurred in the afternoon, coinciding with the period of maximum (westerly) winds. In October, the correlation between the sheared first EOF mode of across-shore velocity, and the first EOF mode of temperature were high. Temperature lagged across-shore velocity by 1.7 hours on average, with maximum temperatures achieved shortly after maximal onshore surface flow. Correlations of across-shore velocity and temperature with surface elevation and alongshore velocity were very weak in October.

[25] A comparison of the time rate of change of temperature and the advective flux in the across-shore and alongshore directions indicates that observed temperature changes in October are well described by across-shore advection. Figure 6 shows time series and scatterplots of the time rate of change of temperature, dT/dt, and the across-shore advective flux, $v_s dT/dy_s$ where the subscript s denotes a coordinate system that is parallel to the bottom and positive upslope, for the lower part of the water column for the October experiment. The close agreement between these terms and the poor agreement with the alongshore advection term, not shown, suggests that temperature changes we observe in the bottom part of the water column are primarily a result of across-shore (up and down-slope) advection. Alongshore advection may have a more important role in May, when alongshore velocities are higher, however our instrument layout for the May experiment does not allow us to accurately calculate spatial gradients in temperature.

[26] For the October measurements, the across-shore density gradient was calculated from the temperature difference between sites 7 and 9 at the same depth below surface (thermistors 5, 6, 7 and 8 m below mean water level). The across-shore near-bottom velocity is well correlated with $(g'H)^{1/2}$, where g' is the reduced gravity calculated from the horizontal temperature difference, and H is the total water depth (Figures 6c and 6d). This balance suggests a conversion of potential energy, due to horizontal density gradients, to kinetic energy in the form of the observed sheared across-shore flow. Our slope (0.08) is significantly less than the theoretical slope (0.25) for a frictionless gravity current [*Benjamin*, 1967; *Simpson*, 1997] and we attribute this difference to substantial energy losses due to bottom and water column drag.

[27] The dominant spectral peak in October was semidiurnal and the observed temperature and across-shore velocity variations are thought to be associated mainly with internal tides. In May the alongshore flow was highly correlated with the across-shore velocity and temperature, the dominant spectral peak was diurnal, maximum eastward velocities occurred in the midafternoon when westerly winds were strongest, and we believe that diurnal wind variations play an important role in driving the observed flow.

4.3. Transport Due to Waves: Stokes Drift

[28] Stokes drift is a slow drift in the direction of propagation of a wave, and arises because particle orbits are not closed for finite amplitude waves [*Kundu*, 1990; *Longuet-Higgins*, 1953]. In order to assess the significance of Stokes drift relative to mean currents for across-shore transport at the field site, the net shoreward Lagrangian transport due to waves was estimated from expressions derived for linear wave theory [*Dean and Dalrymple*, 1991]. Stokes drift spectra were calculated from wave height spectra and were then integrated over all frequencies to obtain the net drift in the direction of wave propagation due to the measured wave field [*Kenyon*, 1969; *Monismith and Fong*, 2004].

[29] For monochromatic waves, the Stokes drift velocity as a function of depth is [*Dean and Dalrymple*, 1991]

$$u(z) = \frac{ga^2k^2 \cosh 2k(h+z)}{\omega \sinh 2kh} \tag{1}$$

where g is the acceleration due to gravity, a is the wave amplitude, k is wavenumber, h is the water depth, ω is the frequency in radians per second, and z is the vertical coordinate (z = 0 at the mean water surface level, positive upward). For a spectrum of wave energy, the contribution to the net Stokes drift in a given frequency band $[f, f + \Delta f]$ is

$$\Delta u = \frac{2gG_{aa}\Delta f k^2 \cosh 2k(h+z)}{\omega \sinh 2kh} \tag{2}$$

since within a given frequency band, $a^2/2 = G_{aa}\Delta f$, where G_{aa} is the wave amplitude spectral density. Note that k, ω, and G_{aa} are all functions of f. If it is assumed that the wave components in different frequency bands are linear and

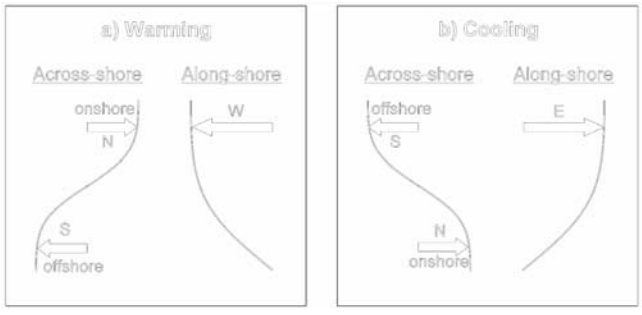

Figure 5. Schematic diagram showing typical across-shore and alongshore flow profiles in May, during periods when the water temperature is (a) warming and (b) cooling.

21562202c, 2007, C2, Downloaded from https://agupubs.onlinelibrary.wiley.com/doi/10.1029/2005JC003430 by University Of North Carolina W, Wiley Online Library on [17/09/2024]. See the Terms and Conditions (https://onlinelibrary.wiley.com/terms-and-conditions) on Wiley Online Library for rules of use; OA articles are governed by the applicable Creative Commons License

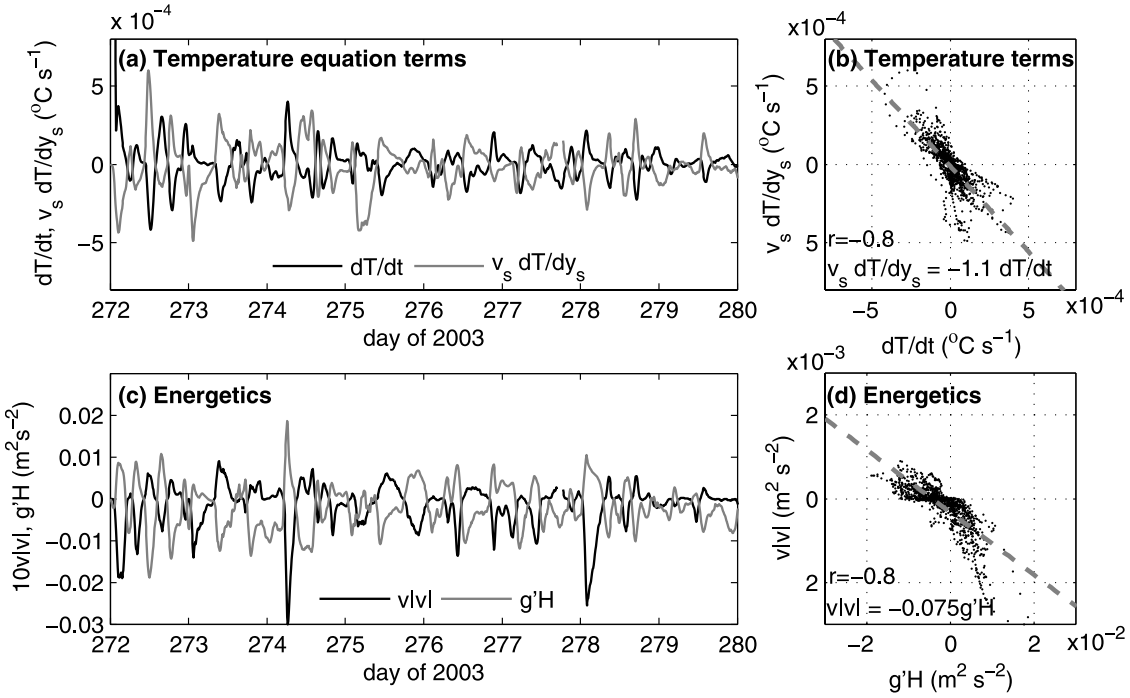

Figure 6. (a) Time series of the time rate of change of temperature (dT/dt) at location 7, averaged over the bottom 3 m of the water column, and the across-shore advective flux (v_s dT/dy_s, where the subscript s denotes a coordinate system that is parallel with the bottom rather than the surface), calculated from velocity and temperature measurements in the bottom 3 m of the water column at locations 7 and 9. (b) Scatterplot of v_s dT/dy_s versus dT/dt. (c) Time series of v|v| and g′H, where v is the average of the across-shore velocity in the lower 3 m of the water column at location 7 and that at location 9, g′ is the reduced gravity calculated from the depth-averaged temperature difference between locations 7 and 9, and H is the average of the water depths at location 7 and location 9. (d) Scatterplot of v|v| versus g′H.

independent, the total Stokes drift is given by the sum over all frequency bands [*Kenyon*, 1969]

$$u(z) = \sum_f \frac{2gG_{aa}k^2 \cosh 2k(h+z)}{\omega \sinh 2kh} \Delta f \tag{3}$$

Similarly it can be shown that the depth-averaged Stokes drift for linear waves is [*Dean and Dalrymple*, 1991; *Kenyon*, 1969]

$$\bar{u}(z) = \sum_f \frac{gG_{aa}k}{\omega h} \Delta f \tag{4}$$

[30] The mean Stokes drift in October, calculated from wave measurements at location 9, was 1.3 cm/s at the surface (0.5 cm/s depth average), and as high as 5 cm/s (2 cm/s depth average) during periods of high wave amplitude. For comparison, the time- and depth-averaged current over the same time period was 2.9 cm/s at location 9, the offshore component being 0.5 cm/s, and the near-surface current was 3.8 cm/s, with an offshore component of 0.8 cm/s. In May, we do not have wave measurements outside the kelp forest; however, the mean Stokes drift calculated from wave measurements at location 1 was 3.2 cm/s at the surface (1.6 cm/s depth average), reaching 6 cm/s during periods with high wave amplitudes (3 cm/s depth average). Stokes drift at the surface was the same at location 1 as at location 9 during the week in October when measurements were made simultaneously at both sites; however, the depth averaged Stokes drift was 50% higher at location 1 than at location 9 during this period due to the shallower water depth. We attribute the higher near-surface Stokes drift estimates in May to the wind wave peak that was present in May, but almost absent in October. In the intermediate and deep water wave regime, higher frequency waves make a greater contribution to Stokes drift for the same wave height, and wind waves fall into this category. During both May and October, the instantaneous current velocity was usually much greater than the instantaneous Stokes drift. However, Stokes drift was comparable with mean current in a time-averaged sense, and may therefore be an important consideration when estimating net across-shore transport over time periods longer than one day.

5. Effect of the Kelp Forest on Hydrodynamics and Transport

5.1. Kelp Forest Structure

[31] Contour plots showing the percentage of the surface area that was covered by kelp canopy, calculated from aerial photographs taken during each experiment, are shown in Figure 7, along with instrument locations. The surface

21562202c, 2007, C2, Downloaded from https://agupubs.onlinelibrary.wiley.com/doi/10.1029/2005JC003430 by University Of North Carolina W, Wiley Online Library on [17/09/2024]. See the Terms and Conditions (https://onlinelibrary.wiley.com/terms-and-conditions) on Wiley Online Library for rules of use; OA articles are governed by the applicable Creative Commons License

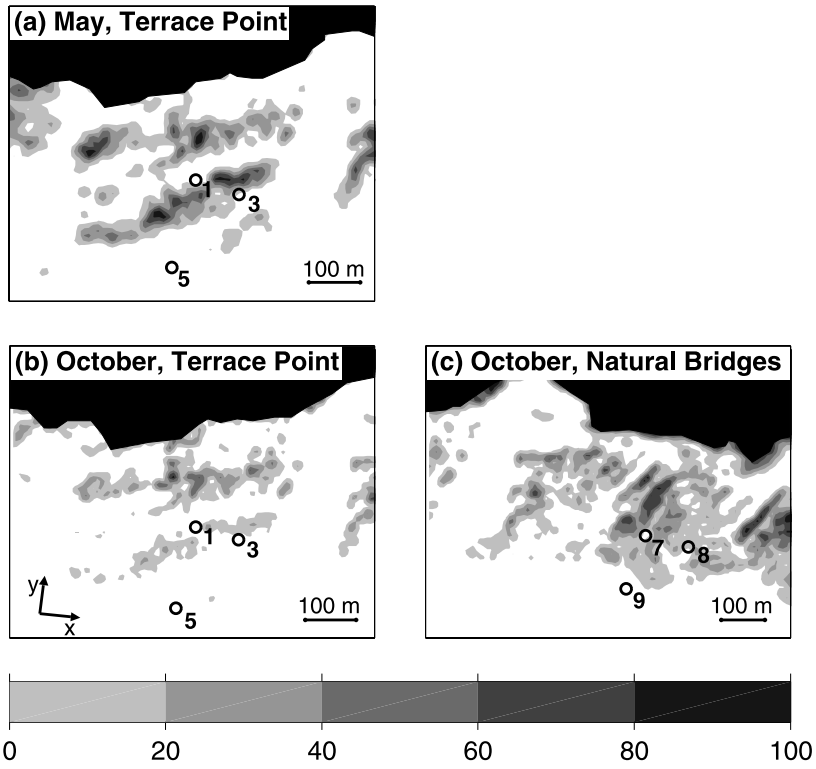

Figure 7. Contour plots of the percent of the surface that was covered with kelp canopy during the two experiments, calculated from color analysis of aerial photographs. Figures correspond to (a) May, Terrace Point, (b) October, Terrace Point and (c) October, Natural Bridges. Land area is masked in black. Instrument locations are numbered. Positive alongshore (x) and positive across-shore (y) directions are drawn on subplot (b).

canopy coverage in May was much higher than that at the same location in October; however, an extra site to the east of Terrace Point (Natural Bridges), where kelp coverage was more continuous, was added for the second experiment. Sites were thus classified as high coverage (October, Natural Bridges), intermediate coverage (May, Terrace Point) and low coverage (October, Terrace Point).

[32] In May, the mean kelp density deduced from diver transects was 5 individuals per 100 m^2 (standard deviation 6 per 100 m^2). In October, the mean kelp density at Terrace Point from diver transects was 6 individuals per 100 m^2 (standard deviation 3 per 100 m^2), and the mean kelp density at Natural Bridges was 9 individuals per 100 m^2 (standard deviation 4 per 100 m^2).

5.2. Effect of the Kelp Forest on Currents

[33] The magnitude of the current within the kelp forest was significantly reduced from that outside the kelp forest, particularly in the alongshore direction. Figure 8 shows time series of alongshore and across-shore velocity, averaged over six bins (3 m) at the top and bottom of the water column, during the October deployment. Note the larger velocities in the alongshore direction outside the kelp forest (location 9), and the significant reduction in velocity magnitude and shear within the kelp forest (location 7). The across-shore flow is affected to a lesser extent. Velocities at location 7, within the kelp forest, are plotted against those at location 9, outside the kelp forest, in Figure 8 and velocity reduction factors have been deduced from the slope of linear fits to these plots. Alongshore velocities within the kelp forest were reduced by a factor of 5 in the upper part of the water column and a factor of 4 in the lower part of the water column, while across-shore velocities were reduced by a factor of 3.5 in the upper part of the water column and 2.2 in the lower part of the water column. We find that this factor is relatively consistent across mean currents, subtidal variations and tidal band variations. At higher frequencies the correlation between different sites dies off significantly.

[34] Comparisons between velocities at different sites, and between the two experiments, indicate that velocity reduction is a function of surface canopy coverage. Scatterplots comparing depth averaged velocities at location 1 and those at location 3 are shown in Figure 9. During the May experiment, mean alongshore velocities at location 3 were larger than those at location 1 when the mean flow was toward the west, while mean alongshore velocities at location 1 were larger when the flow was toward the east. This difference can be attributed to the kelp patch between location 1 and location 3. The difference between velocities at locations 1 and 3 was smaller in October when the kelp canopy in this kelp patch was less dense.

[35] The observed reductions in depth averaged alongshore velocities within the kelp forest are summarized in Table 4, along with the kelp densities from diver transects, and surface canopy coverages determined from aerial photographs. With our present measurements, it is not possible to separate out the effects of kelp from the effects

21562202c, 2007, C2, Downloaded from https://agupubs.onlinelibrary.wiley.com/doi/10.1029/2005JC003430 by University Of North Carolina W, Wiley Online Library on [17/09/2024]. See the Terms and Conditions (https://onlinelibrary.wiley.com/terms-and-conditions) on Wiley Online Library for rules of use; OA articles are governed by the applicable Creative Commons License

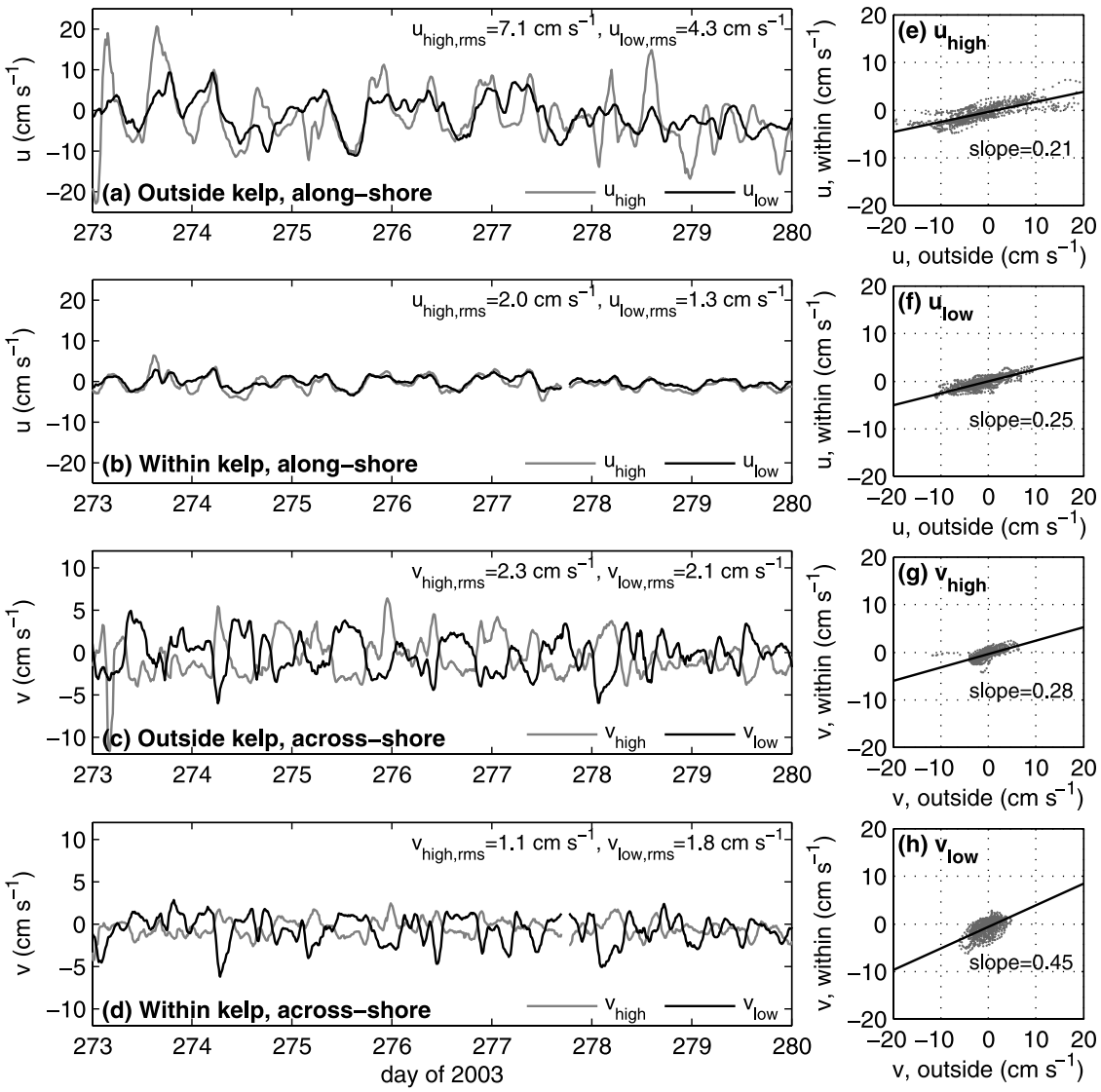

Figure 8. Time series and scatterplots comparing alongshore (u) and across-shore (v) velocities in the upper and lower parts of the water column at sites within (location 7) and outside (location 9) the kelp forest during the October deployment. Time series plots correspond to (a) alongshore velocity, location 9, (b) alongshore velocity, location 7, (c) across-shore velocity, location 9 and (d) across-shore velocity, location 7. Upper water column velocities, shown in grey, are averaged over the top six bins (3 m) and lower water column velocities, shown in black, are averaged over the bottom six bins (3 m). Scatterplots of velocity within the kelp forest versus that outside the kelp forest correspond to (e) upper water column, alongshore velocity, (f) lower water column, alongshore velocity, (g) upper water column, across-shore velocity and (h) lower water column, across-shore velocity.

of bathymetry or variation in bottom friction, or to distinguish flow reduction within a kelp forest from flow acceleration around the outer edge of the kelp forest (B. Gaylord et al., Spatial patterns of flow and their modification within and around a Giant Kelp forest, submitted to *Limnology and Oceanography*, 2006). Nevertheless, we observe clear differences in flow reduction at the same site between May and October that are most likely related to differences in kelp coverage between seasons. Although it is difficult to quantify differences in kelp coverage and extent between the two sites (Terrace Point and Natural Bridges), we note that the longer extent of kelp canopy at Natural Bridges is associated with a greater effect on alongshore velocity than the smaller kelp patch between locations 1 and 3 at Terrace Point.

[36] We are able to directly compare the reductions in variability observed at our location 7 (115 m inshore of the offshore boundary of the Natural Bridges kelp forest) with that observed at Jackson's location M (120 m inshore of the offshore boundary of the Point Loma kelp forest). We observe a factor of 4–5 reduction in 10-min averaged alongshore velocities between locations 7 and 9, based on the slope of the scatterplots in Figure 8. Jackson observed a factor of 2 reduction in alongshore velocities between locations O and M, based on standard deviations of current measurements made at 4-min intervals over the course of

21562202c, 2007, C2, Downloaded from https://agupubs.onlinelibrary.wiley.com/doi/10.1029/2005JC003430 by University Of North Carolina W, Wiley Online Library on [17/09/2024]. See the Terms and Conditions (https://onlinelibrary.wiley.com/terms-and-conditions) on Wiley Online Library for rules of use; OA articles are governed by the applicable Creative Commons License

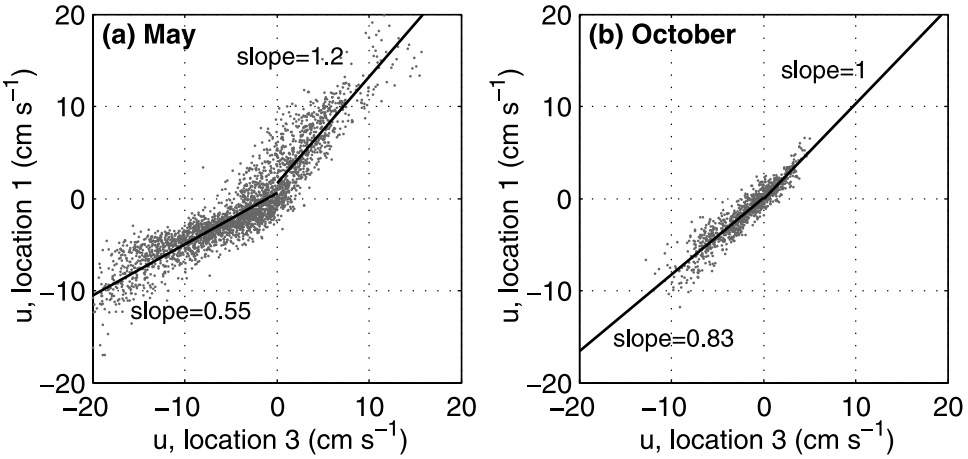

Figure 9. Scatterplots of depth-averaged alongshore velocities at location 1 versus those at location 3 for the two deployments. Plots correspond to (a) May (high surface canopy coverage), and (b) October (low surface canopy coverage).

his 4-week experiment. We find a 2.2–3.6 fold reduction in across-shore velocity between locations 9 and 7, which can be compared with Jackson's reduction factor of 2.2 over similar across-shore distance between his O and M. There are a number of factors that could contribute to the differences between the velocity reductions observed by Jackson and our results. Most notably, our location 7 is in 7 m of water, compared with Jackson's site M, in 17 m of water. If we assume that the majority of drag in kelp forests of this density (0.01–0.1 individuals/m^2) is due to the surface canopy, then the effect of the surface canopy can be modeled as a boundary layer and the drag term in the depth-averaged momentum equations is inversely proportional to water depth. Other potential differences between Jackson's and our experiments include differences in the across-shore exchange of alongshore momentum (v du/dy), and differences in the thickness of the surface canopy.

5.3. Effect of the Kelp Forest on Internal Waves

[37] Temperature spectra for sites within and outside the kelp forest are compared in Figure 10. Temperature variations associated with tidal frequency internal waves were not damped considerably within the kelp forest (Figure 10c), even though the associated across-shore velocities were damped by a factor of 2–3.5 (refer to section 5.2). Temperature variations associated with higher frequency internal waves, however, were reduced within the kelp forest. Characteristic isopycnal displacements and vertical velocities that were observed at location 9, outside the kelp forest (section 4.1), were completely absent at site 7, inside the kelp forest. The damping of these internal waves can be seen in the deviation of the two temperature spectra in the range 0.0001 to 0.01 Hz (Figure 10c). Outside the kelp forest, the high frequency end of the internal wave band clearly coincides with the Brunt-Väisälä frequency (Figure 10b), while inside the kelp forest the energy dies off well below the Brunt-Väisälä frequency (Figure 10a). The dissipation of these waves may contribute to turbulence generation and mixing in the outer part of the kelp forest.

5.4. Effect of the Kelp Forest on Surface Waves

[38] Wave spectra at location 9, offshore of the kelp forest, and location 8, within the kelp forest, were much the same, with the exception of a 30% higher swell wave peak at the shallower site (location 8) that is consistent with normal shoaling. This indicates that swell (period 7–15 s) is not significantly damped by the kelp canopy. There was no distinct wind wave peak (period 4–6 s) in October, therefore we cannot assess the effect of the kelp canopy on wind waves. Waves with periods smaller than 3 seconds were not resolved by our bottom mounted pressure sensor in 10 m of water; however, visual observations suggest that wind ripples are damped by the surface canopy.

[39] In order to assess the importance of onshore transport due to waves compared with Eulerian currents within the

Table 4. Summary of Kelp Density and Surface Canopy Coverage, Along With Observed Reductions in Alongshore Velocity Within the Kelp Forest[a]

	Kelp Density (per 100 m^2)		Canopy Coverage, %		
Deployment, Site	Mean	Standard Deviation	Mean	Standard Deviation	Velocity Reduction
May, Terrace Point	5	6	31	26	1.5–2
Oct, Terrace Point	6	3	5	6	1.1–1.2
Oct, Natural Bridges	9	4	23	16	4–5

[a]Kelp densities are individuals per 100 m^2 calculated from diver transect data. Surface canopy coverage is calculated from aerial photographs. Canopy coverage is the mean percent coverage over a rectangular area with corners formed by locations 1 and 3 at Terrace Point, and a rectangular area centered on location 7 (side lengths 200 m alongshore and 100 m across-shore) at Natural Bridges. Velocity reduction factors are obtained from least squares fits to scatterplots of depth averaged velocities: location 1 versus location 3 at Terrace Point and location 7 versus location 9 at Natural Bridges.

21562202c, 2007, C2, Downloaded from https://agupubs.onlinelibrary.wiley.com/doi/10.1029/2005JC003430 by University Of North Carolina W, Wiley Online Library on [17/09/2024]. See the Terms and Conditions (https://onlinelibrary.wiley.com/terms-and-conditions) on Wiley Online Library for rules of use; OA articles are governed by the applicable Creative Commons License

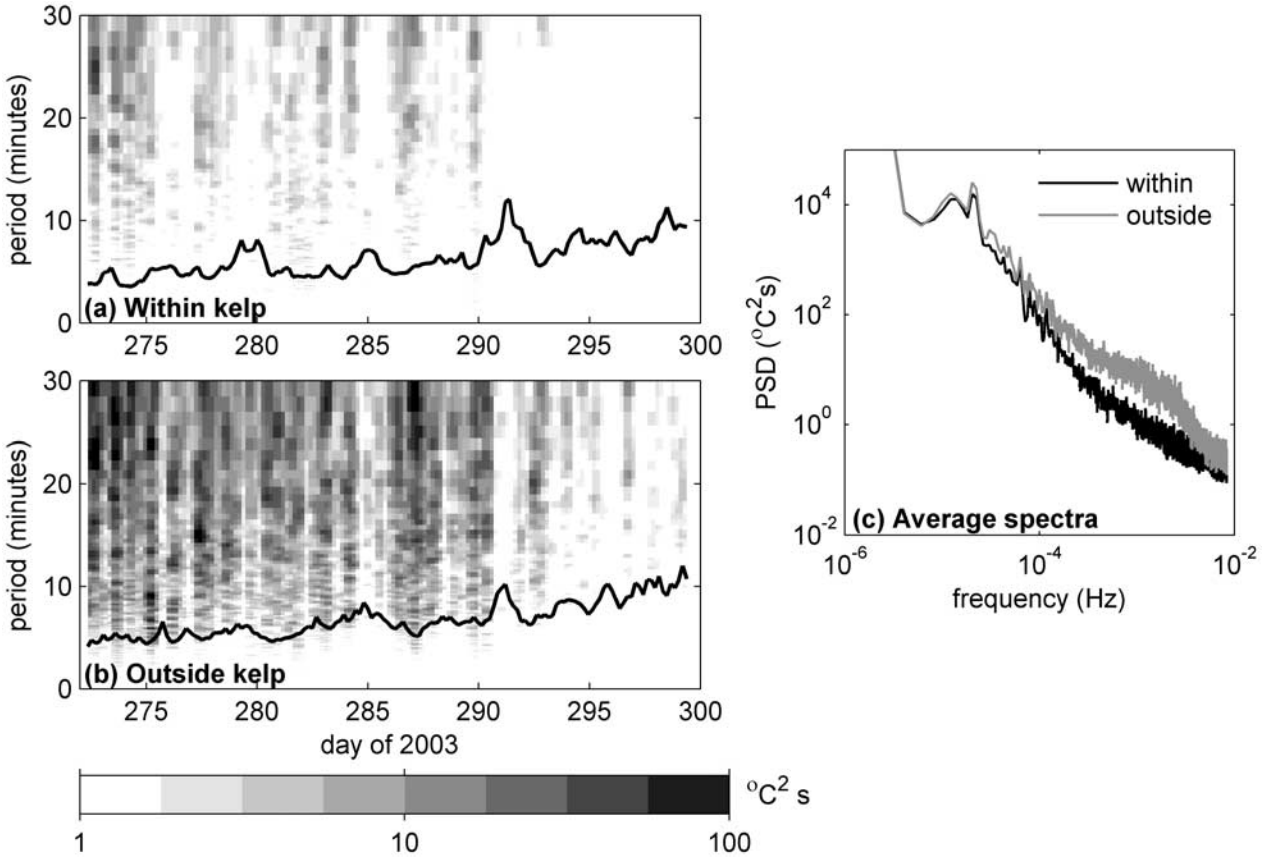

Figure 10. Variation of temperature spectra with time at (a) location 7, within the kelp forest, and (b) location 9, outside the kelp forest, during the October deployment. The solid line corresponds to the Brunt-Väisälä frequency. (c) Average temperature spectra over the full four week deployment at these sites. Spectra shown are averages of the spectra calculated from thermistors at three vertical positions in the midwater column, 5, 6 and 7 m below mean water level.

kelp forest, Stokes drift was calculated from wave height measurements at location 8 using equation (2). As linear wave theory may not provide accurate estimates of Stokes drift within the kelp forest, our goal is only to provide a rough first estimate. Comparisons between Stokes drift estimates and Eulerian velocities measured by the ADCP at location 7 are shown in Figure 11. Within the kelp forest, the magnitude of the instantaneous Stokes drift is typically 20–25% of the magnitude of the instantaneous Eulerian velocity (Figures 11a and 11b), and is often comparable with the across-shore component of the Eulerian velocity. Total velocities and time integrated displacements due to the summation of across-shore currents and Stokes drift are shown in Figures 11c and 11d, respectively. The net across-shore movement of water particles is predicted to be onshore in the upper part of the water column and offshore in the lower part of the water column at this measurement location.

[40] Over long time periods (much greater than one day), the depth-average onshore Stokes transport predicted from linear wave theory closely matches the net depth-average offshore Eulerian drift at this measurement location; however, Stokes drift and offshore Eulerian transport do not agree closely over shorter time scales. The offshore Eulerian flow could be a residual of the tidal flow, due to aspects of the bathymetry or flow deviation around the kelp forest, or it may be related to a wave driven circulation.

5.5. Effect of the Kelp Forest on Turbulence Generation

[41] Richardson numbers calculated from spline interpolated ADCP velocity profiles and temperature profiles are shown in Figure 12. Ten minute averaged velocities and temperatures were used for these calculations. Richardson number (Ri) is defined as the square of Brunt-Väisälä frequency (N^2) divided by the square of the velocity shear (S^2). Richardson numbers greater than 0.25 indicate that local stratification is large enough to suppress turbulence generation by velocity shear. Richardson numbers less than 0.25 indicate times and depths at which vertical mixing due to mean velocity shear could potentially occur. The proportion of calculated Ri that are less than 0.25 (unstable) are plotted versus depth in Figures 12b and 12d. At the site outside the kelp forest, periods during which Ri was less than 0.25 occurred regularly due to velocity shear in the bottom boundary layer and surface boundary layer. Within the kelp forest, Ri remained greater than 0.25 throughout most of the experiment, except for a few periods close to the bed and close to the surface.

[42] Although the strength of the stratification is similar between sites inside and outside of the kelp forest, currents

21562202c, 2007, C2, Downloaded from https://agupubs.onlinelibrary.wiley.com/doi/10.1029/2005JC003430 by University Of North Carolina W, Wiley Online Library on [17/09/2024]. See the Terms and Conditions (https://onlinelibrary.wiley.com/terms-and-conditions) on Wiley Online Library for rules of use; OA articles are governed by the applicable Creative Commons License

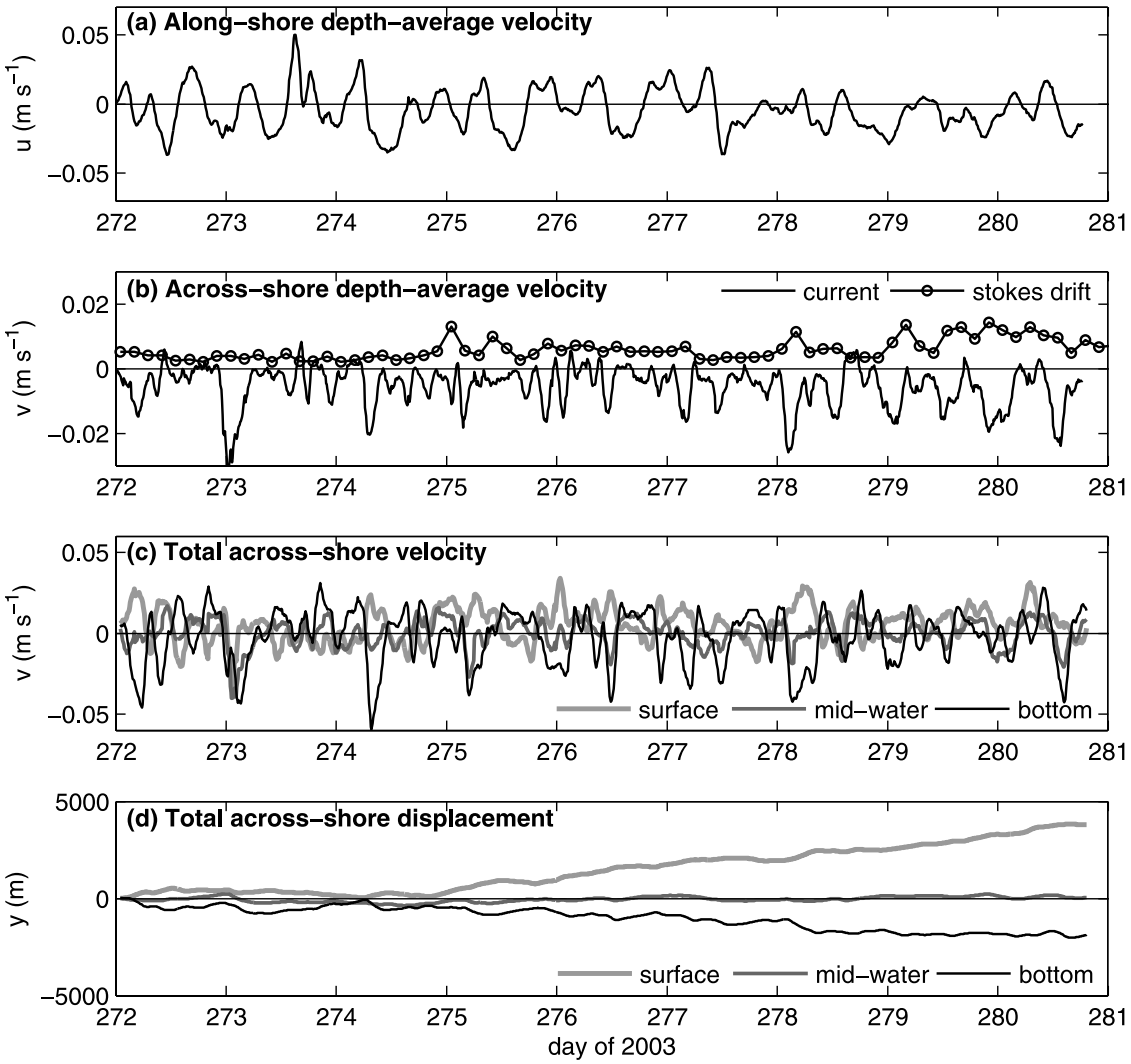

Figure 11. Comparison between Stokes drift calculated from wave height spectra using linear wave theory and currents from ADCP measurements at location 7, within the kelp forest. Plots are (a) depth-averaged alongshore velocity, (b) depth-averaged across-shore velocity and depth-averaged stokes drift, (c) total across-shore particle velocity (the summation of across-shore current and stokes drift) at three heights in the water column, and (d) total Lagrangian across-shore displacement from the beginning of the measurement period, calculated as the cumulative sum over time of the total across-shore velocity in Figure 11c.

are substantially reduced within the kelp forest because it presents a region of high drag to the incident flow (refer to section 5.2). As a result, velocity shear is reduced. We find that Richardson numbers within the kelp forest are generally greater than 0.25 and there is not sufficient velocity shear to overcome local stratification and mix the water column. This result implies that turbulence levels within the kelp forest are low, or that alternative mechanisms exist for generating turbulence and vertical mixing in this system.

6. Summary and Conclusions

6.1. Mechanisms for Horizontal Transport

[43] Transport in the shallow coastal ocean can be driven by surface tides, internal tides and other internal waves, wind and wave-driven circulations, and Lagrangian transport due to surface waves (Stokes drift). All of these mechanisms will be affected by the presence of a region of high drag, such as a kelp forest. Our results indicate that across-shore velocities are less damped by kelp forests than alongshore velocities. Alongshore velocities were damped by a factor (up to 5) that depended on surface canopy coverage and kelp forest density, while across-shore currents were damped by a maximum factor of 3.6. The velocity reductions observed within the kelp forest in the present experiments are up to a factor of two greater than those observed by *Jackson* [1998] over comparable distances. We attribute most of the difference to the significantly shallower water depths of our within-kelp measurement locations (7–9 m) compared with Jackson's measurement locations in the Point Loma kelp forest (14–17 m).

[44] The dominant across-shore flow at the site was a sheared flow that was onshore in one half of the water column and offshore in the other half of the water column,

21562202c, 2007, C2, Downloaded from https://agupubs.onlinelibrary.wiley.com/doi/10.1029/2005JC003430 by University Of North Carolina W, Wiley Online Library on [17/09/2024]. See the Terms and Conditions (https://onlinelibrary.wiley.com/terms-and-conditions) on Wiley Online Library for rules of use; OA articles are governed by the applicable Creative Commons License

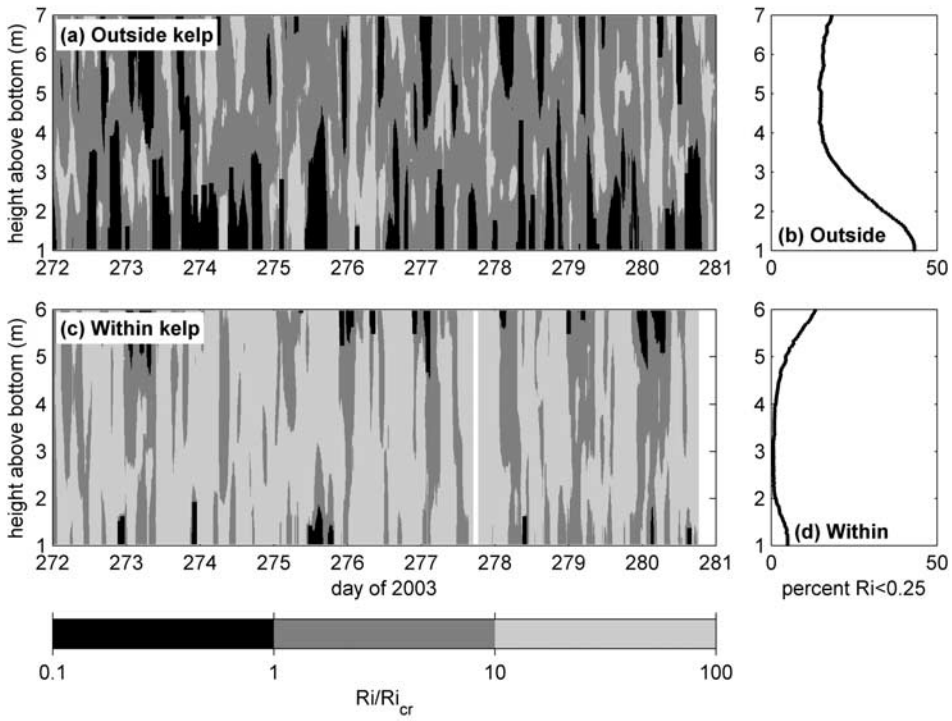

Figure 12. Richardson number versus depth and time at (a) location 9, outside the kelp forest, and (c) location 7, within the kelp forest. Values plotted are Ri/Ri_{cr} where $Ri_{cr} = 0.25$ is the critical Richardson number. Black areas ($Ri < Ri_{cr}$) indicate times and depths at which vertical mixing due to shear in the mean velocity could occur. The proportion of the time that Ri is less than 0.25 is plotted versus height above bottom for (b) location 9 and for (d) location 7.

and reversed on a semidiurnal/diurnal basis. Observed temperature variations were highly correlated with this across-shore flow pattern. During May, an eastward alongshore flow was highly correlated with cooling and onshore flow at the bed, while a westward alongshore flow was associated with warming and offshore flow near the bed. During October the alongshore flow was weak and was uncorrelated with across-shore flow and temperature. Our results from the October experiment indicate that temperature changes near the bed occur primarily due to across-shore advection, and the across-shore flow is driven in a large part by across-shore density gradients. These gradients may be formed as highly nonlinear internal tides approach the coast [e.g., *Rosenfeld*, 1990] or due to wind driven upwelling, and subsequent relaxation, of the thermocline near the shore [e.g., *Rosenfeld*, 1988]. It is thought that diurnal wind patterns are more important in May, while semidiurnal frequency internal tides are present in both May and October. Across-shore excursions near the surface, or near the bed, resulting from the sheared across-shore flow pattern ranged from 100 m to 2 km over a period of 6–12 hours, indicating that it could provide substantial flushing and exchange between the kelp forest and the surrounding coastal ocean on this time scale. As the across-shore flow reverses on a regular (diurnal/semidiurnal) basis, it provides a mechanism for renewal of water in both the lower and upper parts of the water column, even in the absence of vertical mixing within the kelp forest.

[45] While currents are reduced within kelp forests, swell and wind waves pass through relatively unaffected, thus Stokes drift is an important consideration when estimating across-shore transport in these systems. In an instantaneous sense, our Stokes drift estimates were usually exceeded by Eulerian velocities; however, the total onshore flux due to Stokes drift was the same magnitude as the total flux due to the Eulerian velocity in a time-averaged sense. Although our estimates of Stokes drift within the kelp forest were based on linear theory, which may be significantly modified by the interaction of the kelp drag profile with wave orbital velocities, our results highlight the importance of considering Stokes drift when estimating transport rates in wave-affected regions.

6.2. Mechanisms for Turbulence Generation and Vertical Transport

[46] An appropriate model to quantify vertical mixing of scalars within complex physical systems such as kelp forests would be an invaluable tool for biologists, for predicting dispersion distances of larvae and spores [*Gaylord et al.*, 2002], and for estimating nutrient availability to marine organisms [*Hurd*, 2000]. Our results indicate that while turbulent production due to velocity shear in the surface and bottom boundary layers is a major mechanism for turbulence generation in the general coastal environment, Richardson numbers within a kelp forest can remain greater than 0.25 over a large portion of the water column for a large fraction of the time. Velocity shear within the kelp forest at

21562202c, 2007, C2, Downloaded from https://agupubs.onlinelibrary.wiley.com/doi/10.1029/2005JC003430 by University Of North Carolina W, Wiley Online Library on [17/09/2024]. See the Terms and Conditions (https://onlinelibrary.wiley.com/terms-and-conditions) on Wiley Online Library for rules of use; OA articles are governed by the applicable Creative Commons License

our site was seldom sufficient to overcome local stratification and cause vertical mixing because flow velocities, and hence velocity shear, were dramatically reduced. Other mechanisms for turbulence generation in kelp forests may include wake generation behind individual kelp bundles due to their interaction with currents and surface waves [*Nepf et al.*, 1997; *Nepf*, 1999], or turbulence generation due to the breakdown and decay of high frequency internal waves. Alternatively, it is possible that vertically sheared across-shore flows bring nutrients, food particles, larvae and spores to all parts of the water column without a need for substantial vertical mixing within the kelp forest. Characterization of the turbulence field and scalar mixing rates within kelp forests is a challenging problem that requires further work.

[47] **Acknowledgments.** We are endebted to Mark Carr and PISCO for providing the boat time and technical support required for the field experiments. We would like to thank Matthew Reidenbach, Ryan Lowe, Michael O'Donnell, Cary Troy, Nicole Jones and Kristen Davis from the Environmental Fluid Mechanics Laboratory at Stanford, and Patrick Berk, Mike Moss, Selena McMillan and Karah Cox from the Long Marine Laboratory at UC Santa Cruz for their assistance with diving and field deployments. Randolph Skrovan deserves a special mention for the many hours he put into making the deployments happen. Alex Pang and the REINAS project at the University of California, Santa Cruz, provided us with local wind data. We would also like to acknowledge Curt Storlazzi and Mark Carr for their help during the planning stages of the project, and Derek Fong, Jim Hench and Cary Troy for their input and suggestions during the analysis and writing. Funding was provided by the National Science Foundation (CTS-0335346).

References

Bassin, C., L. Washburn, M. Brzezinski, and E. McPhee-Shaw (2005), Submesoscale coastal eddies observed by high frequency radar: A new mechanism for delivering nutrients to kelp forests in the Southern California Bight, *Geophys. Res. Lett.*, *32*, L12604, doi:10.1029/2005GL023017.

Benjamin, T. (1967), Gravity currents and related phenomena, *J. Fluid Mech.*, *31*(2), 209–248.

Breaker, L., and W. Broenkow (1994), The circulation of Monterey Bay and related processes, *Oceanogr. Mar. Biol.*, *32*, 1–64.

Colosi, J., J.F. Lynch, G. Gawarkiewitcz, C.-S. Chui, and A. Scotti (2001), Observations of nonlinear internal waves on the outer New England continental shelf during the summer Shelfbreak Primer study, *J. Geophys. Res.*, *106*(C5), 9587–9601.

Dayton, P. (1985), Ecology of kelp communities, *Ann. Rev. Ecol. Syst.*, *16*, 215–245.

Dean, R., and R. Dalrymple (1991), *Water Wave Mechanics for Engineers and Scientists*, World Sci., Hackensack, N. J.

Drake, P., M. McManus, and C. Storlazzi (2005), Local wind forcing of the Monterey Bay area inner shelf, *Cont. Shelf Res.*, *25*, 397–417.

Elwany, M., W. O'Reilly, R. Guza, and R. Flick (1995), Effects of southern California kelp beds on waves, *J. Waterw. Port Coastal Ocean Eng.*, *121*(2), 143–150.

Gaylord, B., D. C. Reed, P. T. Raimondi, L. Washburn, and S. McLean (2002), A physically based model of macroalgal spore dispersal in the wave and current-dominated nearshore, *Ecology*, *83*(5), 1239–1251.

Gaylord, B., M. Denny, and M. Koehl (2003), Modulation of wave forces on kelp canopies by alongshore currents, *Limnol. Oceanogr.*, *48*(2), 860–871.

Graham, M. (2003), Coupling propagule output to supply at the edge and interior of a Giant Kelp forest, *Ecology*, *84*(5), 1250–1264.

Hurd, C. (2000), Water motion, marine macroalgal physiology, and production, *J. Phycol.*, *36*, 453–472.

Jachec, S., O. Fringer, M. Gerritsen, and R. Street (2006), Numerical simulation of internal tides and the resulting energetics within Monterey Bay and the surrounding area, *Geophys. Res. Lett.*, *33*, L12605, doi:10.1029/2006GL026314.

Jackson, G. (1984), Internal wave attenuation by coastal kelp stands, *J. Phys. Oceanogr.*, *14*, 1300–1306.

Jackson, G. (1998), Currents in the high drag environment of a coastal kelp stand off California, *Cont. Shelf Res.*, *17*(15), 1913–1928.

Jackson, G., and C. Winant (1983), Effect of a kelp forest on coastal currents, note, *Cont. Shelf Res.*, *2*(1), 75–80.

Kenyon, K. (1969), Stokes drift for random gravity waves, *J. Geophys. Res.*, *74*, 6991–6994.

Kundu, P. (1990), *Fluid Mechanics*, Elsevier, New York.

Kunze, E., L. Rosenfeld, G. Carter, and M. Gregg (2002), Internal waves in Monterey submarine canyon, *J. Phys. Oceanogr.*, *32*, 1890–1913.

Langstroth, L., and L. Langstroth (2000), *A Living Bay: The Underwater World of Monterey Bay*, Univ. of Calif. Press, Berkeley.

Leichter, J. J., S. R. Wing, S. L. Miller, and M. W. Denny (1996), Pulsed delivery of subthermocline water to Conch Reef (Florida Keys) by internal tidal bores, *Limnol. Oceanogr.*, *41*(7), 1490–1501.

Leichter, J. J., G. Shellenbarger, S. J. Genovese, and S. R. Wing (1998), Breaking internal waves on a Florida (USA) coral reef: a plankton pump at work?, *Mar. Ecol. Prog. Ser.*, *166*, 83–97.

Lerczak, J. A., C. D. Winant, and M. C. Hendershott (2003), Observations of the semidiurnal internal tide on the southern California slope and shelf, *J. Geophys. Res.*, *108*(C3), 3068, doi:10.1029/2001JC001128.

Longuet-Higgins, M. (1953), Mass transport in water waves, *Philos. Trans. R. Soc. London*, *245*, 535–581.

Monismith, S., and D. Fong (2004), A note on the potential transport of scalars and organisms by surface waves, *Limnol. Oceanogr.*, *49*(4), 1214–1217.

Nepf, H. (1999), Drag, turbulence, and diffusion in flow through emergent vegetation, *Water Resour. Res.*, *35*(2), 479–489.

Nepf, H., J. Sullivan, and R. Zavistoski (1997), A model for diffusion within emergent vegetation, *Limnol. Oceanogr.*, *42*(8), 1735–1745.

Petruncio, E., L. Rosenfeld, and J. Paduan (1998), Observations of the internal tide in Monterey canyon, *J. Phys. Oceanogr.*, *28*, 1873–1903.

Piñeda, J. (1994), Internal tidal bores in the nearshore - warm-water fronts, seaward gravity currents and the onshore transport of neustonic larvae, *J. Mar. Res.*, *52*(3), 427–458.

Rosenfeld, L. (1988), Diurnal period wind stress and current fluctuations over the continental shelf off northern California, *J. Geophys. Res.*, *93*(C3), 2257–2276.

Rosenfeld, L. (1990), Baroclinic semidiurnal tidal currents over the continental shelf off northern California, *J. Geophys. Res.*, *95*(C12), 22,153–22,172.

Rosenfeld, L., and R. Beardsley (1987), Barotropic semidiurnal tidal currents of northern California during the Coastal Ocean Dynamics Experiment (CODE), *J. Geophys. Res.*, *92*(C2), 1721–1732.

Simpson, J. (1997), *Gravity Currents in the Environment and the Laboratory*, Cambridge Univ. Press, New York.

Storlazzi, C., M. McManus, and J. Figurski (2003), Long-term high frequency current and temperature measurements along central California: insights into upwelling/relaxation and internal waves on the inner shelf, *Cont. Shelf Res.*, *23*, 901–918.

Utter, B., and M. Denny (1996), Wave-induced forces on the Giant Kelp *Macrocystis pyrifera* (Agardh): field test of a computational model, *J. Exper. Biol.*, *199*, 2645–2654.

Zimmerman, R., and J. Kremer (1984), Episodic nutrient supply to a kelp forest ecosystem in southern California, *J. Mar. Res.*, *42*, 591–604.

J. Grover, Institute of Marine Sciences, University of California, Santa Cruz, CA 95060, USA.

J. R. Koseff, S. G. Monismith, and J. H. Rosman, Environmental Fluid Mechanics Laboratory, Civil and Environmental Engineering, Stanford University, Stanford, CA 94305-4020, USA. (jrosman@stanford.edu)

21562202c, 2007, C2, Downloaded from https://agupubs.onlinelibrary.wiley.com/doi/10.1029/2005JC003430 by University Of North Carolina W, Wiley Online Library on [17/09/2024]. See the Terms and Conditions (https://onlinelibrary.wiley.com/terms-and-conditions) on Wiley Online Library for rules of use; OA articles are governed by the applicable Creative Commons License